Numerical model of Lamb wave propagation in the tapered septal wall of the heart

Alberico Sabbadini, Annette Caenen, Hendrik J. Vos, Nico de Jong, and Martin D. Verweij

Citation: Proc. Mtgs. Acoust. **39**, 020003 (2019); doi: 10.1121/2.0001226
View online: https://doi.org/10.1121/2.0001226
View Table of Contents: https://asa.scitation.org/toc/pma/39/1
Published by the Acoustical Society of America

ARTICLES YOU MAY BE INTERESTED IN

Acoustic radiation force and torque on inhomogeneous particles in the Born approximation
Proceedings of Meetings on Acoustics **39**, 045007 (2019); https://doi.org/10.1121/2.0001255

Music Information Retrieval – the Impact of Technology in Art, Crowdsourcing, Big Data, and the Cloud
Proceedings of Meetings on Acoustics **39**, 035005 (2019); https://doi.org/10.1121/2.0001225

Practical realisation of an active acoustic metamaterial building block
Proceedings of Meetings on Acoustics **39**, 045006 (2019); https://doi.org/10.1121/2.0001229

Laboratory simulations of conversation scenarios: questionnaire results from patient and partner
Proceedings of Meetings on Acoustics **39**, 050004 (2019); https://doi.org/10.1121/2.0001245

Modelling Lamb waves in the septal wall of the heart
The Journal of the Acoustical Society of America **146**, 3070 (2019); https://doi.org/10.1121/1.5137654

Application of elastic parabolic equation solutions to calculation of acoustic reverberation in ice-covered underwater environments
Proceedings of Meetings on Acoustics **39**, 022002 (2019); https://doi.org/10.1121/2.0001210

Volume 39 http://acousticalsociety.org/

178th Meeting of the Acoustical Society of America

San Diego, California

2-6 December 2019

Biomedical Acoustics: Paper 5aBA8

Numerical model of Lamb wave propagation in the tapered septal wall of the heart

Alberico Sabbadini
Department of Applied Sciences, Acoustical Wavefield Imaging, ImPhys, Faculty of Applied Science, Delft University of Technology, Delft, Zuid Holland, 2628CJ, NETHERLANDS; a.sabbadini@tudelft.nl

Annette Caenen and Hendrik J. Vos
Biomedical Engineering, Department of Cardiology, Erasmus MC, University Medical Center Rotterdam, Rotterdam, Zuid Holland, NETHERLANDS; annette.caenen@ugent.be, h.vos@erasmusmc.nl

Nico de Jong and Martin D. Verweij
Acoustical Wavefield Imaging, ImPhys, Faculty of Applied Science, Delft University of Technology, Delft, Zuid Holland, NETHERLANDS; nicolaas.dejong@tudelft.nl; m.d.verweij@tudelft.nl

Shear Wave Elastography (SWE) has been proposed to investigate cardiac health by non-invasively monitoring tissue stiffness. Previous work has shown that the plate-like geometry of the Interventricular Septum (IVS) may result in a dispersion similar to Lamb waves, complicating the link between shear wave speed and cardiac stiffness. However, the IVS is not a simple plate, e.g., its thickness tapers across its length. We have used 2-D Finite Element simulations to investigate the effects of tapering on Lamb waves. The model consists of an elastic slab immersed in water, with a thickness decreasing smoothly in space from 9 to 3 mm. Pulses with low (0–80 Hz) and high (0–700 Hz) frequency contents were used to excite natural and acoustic radiation force induced waves. The results show that natural waves can decelerate by up to 20% during propagation, leading to ambiguities in speed estimation. Moreover, neglecting tapering when fitting their dispersion curves can introduce errors in shear modulus estimation by up to 30%. In contrast, fits performed on waves with high frequency content yielded shear modulus estimations with < 5%. These results suggest that septal geometry can affect cardiac stiffness estimation performed by SWE, especially when natural waves are employed.

Published by the Acoustical Society of America

© 2020 Acoustical Society of America. https://doi.org/10.1121/2.0001226

1. INTRODUCTION

Over the past decades, shear wave elastography (SWE) has been under investigation as a medical diagnostic technique to determine non-invasively the stiffness of internal organs.[1–3] In particular, in the field of cardiac imaging,[4–8] SWE could provide a way to monitor cardiac stiffness throughout its cycle, which is a relevant parameter in the diagnosis of heart failure.[9,10]

Two main cardiac SWE approaches currently under investigation, consist of ultrasonically tracking waves that have been generated either by an acoustic radiation force (ARF),[11–14] or by natural physiology of the heart, such as aortic valve closure (AVC).[7,15–18] In both cases, the waves are typically tracked during their propagation along the Interventricular Septum (IVS).

The interpretation of wave speed measurements in terms of stiffness is not straightforward. The simple relation $\rho c^2 = G$ (where ρ is the density of mass, c is the bulk shear speed, and G the shear modulus) – commonly assumed in SWE measurements – cannot be applied directly: waves traveling along the heart walls have been found[4,19–22] to show a dispersive behavior akin to that of Lamb waves. These guided waves are characterized by two infinite sets of modes (symmetric and antisymmetric) that propagate at speeds depending on frequency, as well as stiffness and thickness of the medium itself.[23] Moreover, since the IVS separates two chambers filled with blood, it is often approximated as a fluid-loaded plate. The dispersive behaviour, thus, also depends on the medium properties of the fluid that surrounds the plate.[23,24]

Some cardiac SWE studies[20] have accounted for this dispersive behaviour by analysing in the Fourier domain waves at various frequencies, from which the experimental characteristic dispersion curves can be reconstructed. The shear modulus was then extracted by fitting a theoretical dispersion curve of a Lamb wave to the experimental curves.

The IVS, however, is not a straight, flat slab of muscle: its thickness, in fact, can vary by a factor 3 from the equatorial point to the apex.[25] Such a variation is expected to have a significant impact on the guided waves propagating along it, especially at lower frequencies, where zero-order modes depend strongly on the frequency-thickness product. Moreover, it has been shown that a waveguide with a slowly varying thickness can cause reflections and mode conversions when the thickness becomes that small that cut-off of a certain mode is reached.[26–28] To the best of our knowledge, however, no cardiac SWE has studied systematically the effect of thickness variations on wave speed measurements.

The purpose of the present work is to determine the relevance of precise information about the IVS thickness variations for cardiac SWE measurements.

2. METHODS

A. CONFIGURATION

Our numerical model was implemented in Abaqus CAE (Abaqus Inc., Providence, RI, U.S.A.), a Finite Element simulation software that has already been validated for modelling guided waves in biological tissue.[20,29] The IVS was modelled as a 2D plate, with total length $L = 8$ cm (effectively reduced to 4 cm in the numerical model thanks to symmetric boundary conditions), and thickness varying linearly from 9 mm to 3 mm,[24] as shown in Fig. 1. On three sides, the plate was surrounded by a 4 cm thick layer of water.

The plate was considered to be elastic and isotropic, with Poisson's ratio $\nu = 0.49999$ and density $\rho = 1045$ kg/m^3. The Young's modulus was chosen to be $E = 9$ kPa, representing the cardiac muscle in its diastolic phase[14] with a bulk shear wave speed of 1.694 m/s. The water was modelled with acoustic elements, with a density of 1000 kg/m3 and a bulk modulus of 2.2 GPa, resulting in a bulk compressional wave speed of 1483 m/s.

SIMULATIONS

The simulation setup is shown in Fig. 1. The simulations were run using an explicit solver, with mesh size of 0.2 mm, allowing sampling of frequencies up to 600 Hz with at least 25 points per wavelength. The solution computed by Abaqus was then sampled in time-steps of 0.038 ms, allowing at least 45 samples per period for these frequencies. Symmetric boundary conditions were applied along the y-axis, i.e. at the left side of the plate, resulting in symmetry in the x-direction. Abaqus "TIE" constraints were introduced to couple the motion of the plate boundaries to that of the water domain boundaries, preventing relative motions. The outer boundaries of the water domain were implemented with "non-reflecting acoustic boundaries" conditions, to prevent reflections.

In order to study both ARF and AVC waves, two Gaussian pulses were modelled with the 'smooth step' function in Abaqus, with total duration of 2 ms and 10 ms. These pulses described the displacement in the y-axis direction of the left side of the plate, corresponding to two transverse waves with full width at half maximum frequency contents of around 100 and 500 Hz respectively, mimicking the frequencies that can be observed in natural and ARF-induced waves, respectively. The simulations modelled the propagation of the waves for 0.04 seconds, roughly the time that it would take for one pulse to reach the opposite side of the plate.

DATA ANALYSIS

The transverse displacement of the propagating wave at every element and at every time-step was stored in a data file that was subsequently read by a Matlab (version r2018b, MathWorks, Natick, MA, U.S.A.) program for analysis. The displacement data was then interpolated across an 2.2 cm long m-line (a virtual line of receivers), with interpolation grid-spacing of 50 μm. In the analysis of the tapered plate, the m-line was positioned at depth equal to 10% of the thickness. A Radon Sum algorithm was applied to this data to determine the trajectory of the wave, of which the time derivative yields the propagation speed.

The data extracted from a single m-line was further processed with a Tukey window and converted in the frequency-wave number (*f-k*) domain by means of a 2D Fast Fourier Transform, where the dispersion curves correspond to the areas of maximum amplitude. The bulk shear speed of the wave (i.e. the speed at which the shear wave would travel in a bulk material, which is directly connected to the shear modulus) was then estimated by comparing the zero-order antisymmetric dispersion curve (A0) from the simulations with theoretical curves and identifying which parameters would generate the best fit. The Root Mean Squared Percentage Difference (RMS-PD) between the simulated and theoretical curve, computed along the wavenumber axis, was used to quantify the quality of the fit.

Finally, the shear speeds extracted from the space-time (*x-t*) and *f-k* data were converted into values of shear modulus G by computing $G = \rho c^2$, where ρ is the density of mass of the plate and c is the measured shear speed. We point out that the equation holds only when c is the bulk shear speed in the medium, – which is not the speed at which the A0 mode propagates – and therefore it is not the speed observed in the *x-t* data. However, this is the relation employed in most cardiac SWE studies, thus it is useful to assess the error it may introduce.

VALIDATION OF NUMERICAL APPROACH

In order to validate the numerical settings of our simulation, we first ran simulations for a 4 cm long flat slab with constant thickness of 9 mm. The elastic properties of the slab were as described above, corresponding to a bulk shear wave speed of 1.694 m/s. During validation, the wave trajectory was extracted from two m-lines, one in the centre of the slab, the other near the top surface, in order to assess eventual differences.

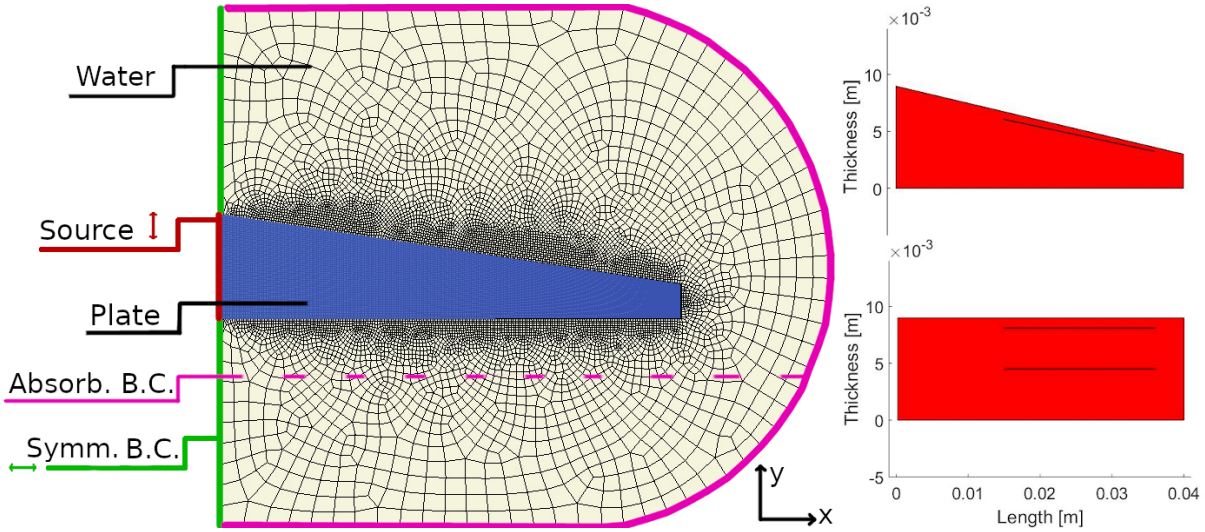

Figure 1: The simulation setup. On the left the numerical FE model is shown, with the plate highlighted in blue and the water in grey. The top right image depicts the plate with a linear thickness decrease and the m-line (in black) on which the data was recorded. The bottom right image shows the flat plate used to validate the numerical approach, and the two m-lines considered (in black).

3. RESULTS

In Fig. 2, the simulation of an ARF-generated wave can be seen in *x-t* and *f-k* domains, as would be recorded on a 2.2 cm long m-line placed at a depth of 0.9 mm in a 4 cm long flat slab. The superimposed white lines represent, respectively, the trajectory of the wave as estimated by the Radon Sum, and the theoretical dispersion curve of the A0 mode of a Lamb wave in the 9 mm thick fluid-loaded plate. The RMS-PD between simulated and theoretical dispersion curve is 1.4%, confirming the reliability of the numerical settings employed in our model. The wave trajectory estimated in the XT domain plot (see left panel of Fig. 1) yields a wave propagation speed of 1.43 m/s.

The left panel of Fig. 3 shows the propagation of the same wave in *x-t* domain, but now recorded on an m-line at the centre of the plate (at a depth of 4.5 mm). It can be seen that, when the wave is tracked along the centre of the plate, the trajectory of the propagation appears 'fragmented', due to the interference of multiple modes. This can also be observed in the right panel, which shows the *f-k* representation of the data and the theoretical dispersion curves corresponding to the simulated plate: the energy of the wave is distributed over two propagation modes, A0 and A1. This is not surprising, considering that the wave contains both frequencies in which only A0 can exist, and ones in which A1 can also be present at that depth.

Simulated data for the waves propagating in a tapered plate with linear thickness decrease are presented in Figs. 4-5. To observe the A0 mode without interference from the A1 mode, the waves were recorded along the virtual m-line close to the top surface of the plate.

Figure 4 shows the two simulated waves (ARF- and AVC- generated) in *x-t* domain. The white lines show the space-time trajectory of the propagating wave. It is evident, however, that a single straight line cannot fit the entire propagation of the wave corresponding to AVC sources, because the trajectory in space-time is curved. In the figure, we show that at least two different lines can fit two sections of the trajectory, i.e. the first and second half of the propagation path, with two different inclinations, which correspond to speeds of 1.24 m/s and 1.03 m/s respectively. The speed of the ARF-generated wave, on the other hand, displays a constant value of 1.30 m/s

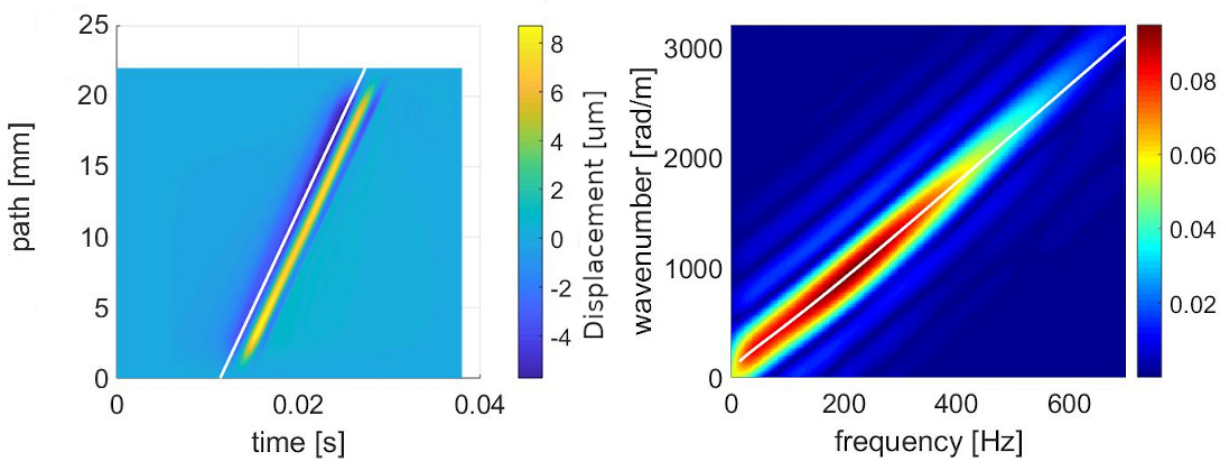

Figure 2: Wave propagation recorded on a 2.2 cm long m-line in a 4 cm long, 9 mm thick flat plate, at a depth of 0.9 mm. On the left image the wave is represented in the* x-t *domain, and the white line shows a Radon Sum estimation of the trajectory of the wave. On the right image, the wave is represented in the* f-k *domain, and the white line represents the theoretical A0 dispersion curve for a plate in water with the same geometry and medium properties. The color scheme represents the magnitude of the Fourier-transformed displacement recorded along the m-line.

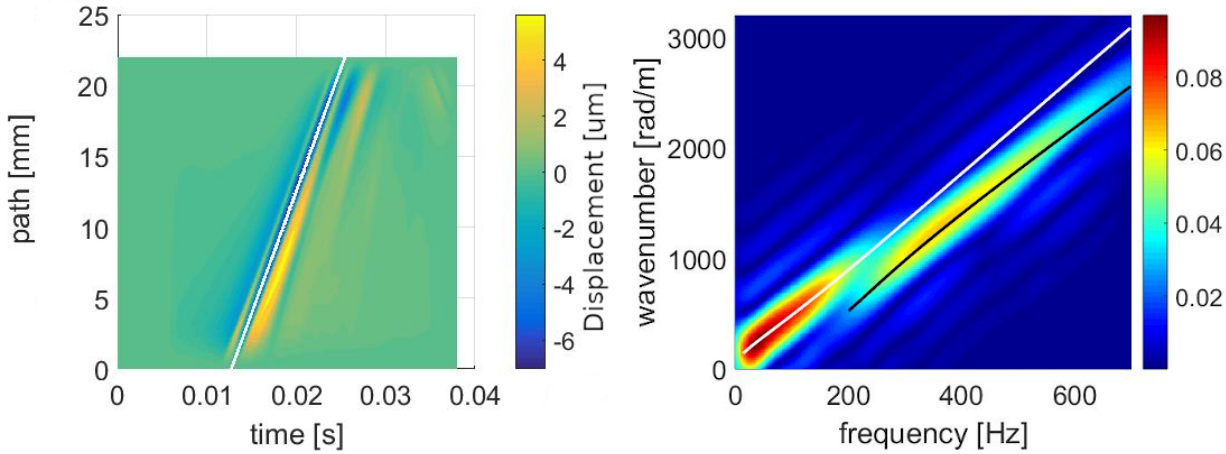

Figure 3: Wave propagation recorded on a 2.2 cm long m-line in a 4 cm long, 9 mm thick flat plate, at a depth of 4.5 mm. On the left image the wave is represented in the* x-t *domain, and the white line shows a Radon Sum estimation of the trajectory of the wave. On the right image, the wave is represented in the* f-k *domain, and the white and black lines represents, respectively, the A0 and A1 theoretical dispersion curves for a plate in water with the same geometry and medium properties. The color scheme represents the magnitude of the Fourier-transformed displacement recorded along the m-line.

Figure 5 shows the propagation data, for the same slab with linear tapering, transformed into *f-k* domain. The superimposed dashed lines show where the dispersion curves would be in a 9 mm plate with E = 9 kPa; the full lines represent the theoretical dispersion curves of a 6 mm plate with E = 9 kPa. It can be seen that the theoretical dispersion curves for a 6 mm plate with are in better agreement with the simulated data. This is also shown quantitatively in Table 1. The value of 6 mm was chosen as a representative of the average

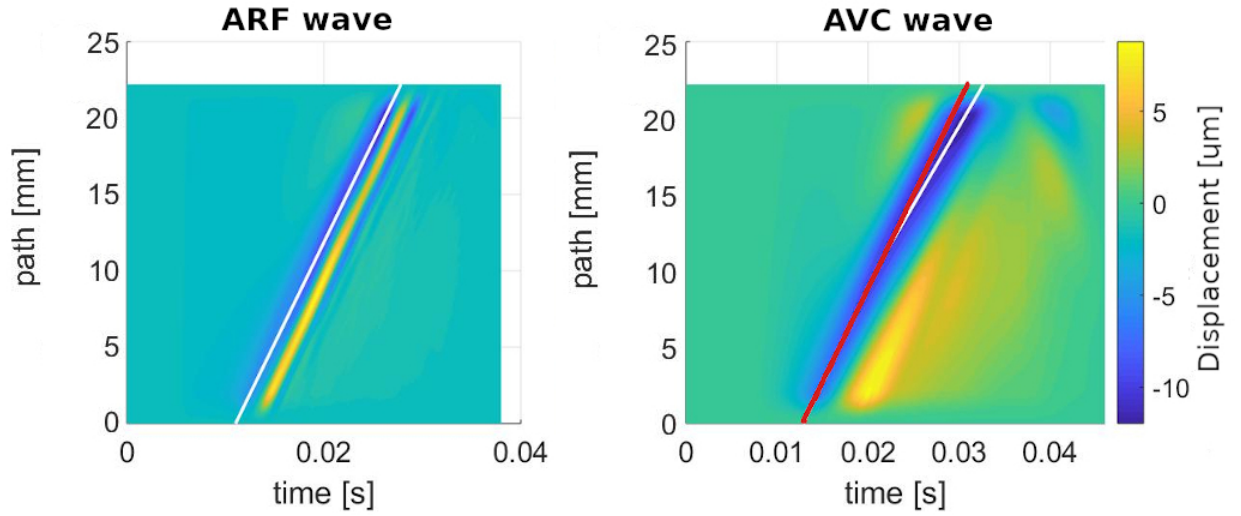

Figure 4: Space-time propagation of ARF- and AVC-generated waves in a plate with linear tapering between 9 and 3 mm. The white and red lines show the Radon Sum estimation of the wave trajectories. For the AVC-generated wave, the red line is obtained by applying the Radon Sum to the first half of the propagation (path 0-0.011 m), and the white line by applying the algorithm to the second half (path 0.011-0.022 m

thickness of the plate (which tapers uniformly between 9 and 3 mm).

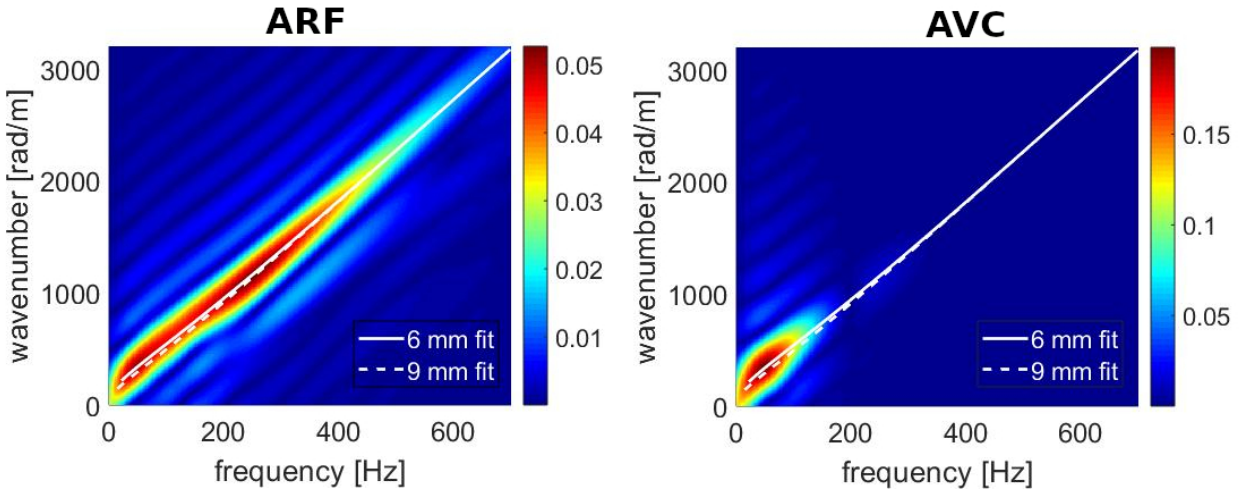

Figure 5: Frequency-wavenumber domain representation of the wave propagation in the tapered slab. The dashed white line represents the theoretical dispersion curve for the A0 mode of a 9 mm thick flat plate, while the full white line shows the theoretical A0 curve of a 6 mm thick flat plate. The color scheme represents the magnitude of the Fourier-transformed displacement recorded along the m-line.

Finally, we show in Table 2 a comparison between the values of shear modulus G that can be extracted by fitting the A0 theoretical curves for a 6 mm and a 9 mm plates to the curve found for the simulated tapered plate. The values are reported in terms of percentage difference between the estimated G and the input value of G in the simulation.

	RMS-PD when fitting with flat plate	
Excitation type	**9 mm plate**	**6 mm plate**
ARF (50-400 Hz)	5.2 %	0.8 %
AVC (20-200 Hz)	14.5 %	1.0 %

Table 1: RMS-PD values for A0 simulated curve of tapered plate fitted with theoretical A0 curves for 6 mm and 9 mm flat plates, for ARF- and AVC-generated waves.

	Deviation of G when fitting with flat plate	
Excitation type	**9 mm plate**	**6 mm plate**
ARF (50-400 Hz)	-5.0 %	-1.4 %
AVC (20-200 Hz)	-29.7 %	-0.2 %

Table 2: Comparison of shear moduli G extracted by fitting the simulated A0 mode of the tapered plate and finding the curves with minimum RMS-PD for flat plates of thickness 6 mm and 9 mm, for ARF- and AVC-generated waves. The deviation of G is expressed here in terms of percentage difference with respect to the input value of G in the simulations.

4. DISCUSSION

In this work we have shown the numerical results for the effects that a linear thickness variation of a plate – mimicking realistic IVS geometries – can have on SWE measurements of medium properties.

Previous studies[26–28] had focused on the effects of tapering on the propagation of waves with relatively high frequencies, where higher order symmetric and antisymmetric modes were present. These higher order modes only appear above well defined values of the frequency-thickness product, and were shown to reflect or convert into lower order modes when the thickness was reduced sufficiently. In contrast, the waves that are studied in cardiac SWE have relatively low frequency content and are mainly characterized by the zero-order modes, which exist at all frequency-thickness products, and the A1 mode, which would not reach its frequency-thickness cut-off value in realistic cardiac geometries (the propagating wave would have to be recorded entirely after a factor 3 thickness reduction). At first glance, it may seem that Fig. 3 displays mode conversion. However, it is important to notice that this is not the case, and, in fact, both A0 and A1 are present simultaneously in Fig. 3. The amplitude of the displacement of each Lamb mode follows a distribution that depends on both the depth and the frequency-thickness product, even in flat plates;[23] the plot in Fig. 3 simply shows that the amplitude distribution of the A0 mode goes to zero for frequencies higher than $\approx$ 200 Hz at the depth of 4.5 mm, whereas closer to the surface, as shown in Fig. 2, the amplitude remains above zero for frequencies up to $\approx$ 600 Hz.

Nevertheless, the thickness variation introduces effects that can be very relevant for cardiac SWE, especially for natural waves (which are more heavily affected by dispersion due to their low frequency contents). First of all, using the shear wave speed obtained from time-domain data in the equation for the bulk shear wave speed will always yield underestimated values of shear modulus G; this happens because the phase speed of the wave in a slab is, in fact, always lower than the bulk shear speed from which G can be derived. Moreover, tapering introduces a clear deceleration of the shear wave at lower frequencies. Due to this deceleration, multiple values of speed may be extracted from the same measurement of AVC-induced waves. In the simulated data we report, fitting the first half of the wave propagation yields a propagation

speed of 1.24 m/s, which is 20% higher than the propagation speed of 1.03 m/s found by fitting the second half. This results in a variation of about 40% in the two corresponding values of G (1.6 kPa and 1.1 kPa). Notably, both values of G are lower than the one that can be extracted from tracking ARF-generated waves (1.8 kPa), and all are lower than the input value (3.0 kPa), reaching in the worst case a variation of 64% between input and extracted G. In comparison, estimating G from the time-domain data for a 9 mm flat plate and the equation for the bulk shear wave speed would give G = 2.0 kPa, i.e. an underestimation of about 33%. From these results, we conclude that tapering of the septal wall may introduce a significant additional error in the stiffness estimation based on time-domain data.

A natural way of extracting G for a plate is to Fourier transform the *x-t* data into the *f-k* domain, where the simulated dispersion curve can be fitted by theoretical curves to yield medium properties. However, as we have shown with our simulations, thickness variations directly affect the dispersive behaviour the waves, both natural and ARF-induced. Theoretically speaking, it doesn't make sense to talk about Lamb dispersion curves in plates of varying thicknesses. As a practical attempt to extract medium properties, however, it may be useful to fit the known curves of fluid-loaded flat plates to the simulation data. In this context, as it is shown by Tables 1 and 2, it becomes important to take into account the specific geometry of the septal wall (or plate) under investigation. In our results, we have shown that fitting based on the average thickness of the tapered plate yielded more accurate results, especially when considering lower frequencies. However, we would like to stress that using the average thickness is only an approximation, and it remains to be investigated how well it performs for different geometries (e.g. convex or concave tapering).

As has been recently reported by Keijzer et al.,[8] the measurements of shear wave speed of AVC-generated waves reported in literature show a variability – within each study - of approximately 20%; the maximum variability between the studies mentioned in that paper is approximately 40%. As we have shown, propagation in tapered media can also introduce a speed variability in the order of 20%. Based on this result, we hypothesize that the septal wall shape could contribute to the variability of shear speeds reported in literature, and we suggest that accounting for the specific geometry of the septum during data analysis may help in reducing the variability of shear wave speed results.

It is also important to notice that, compared to actual cardiac settings, we made several simplifications in our models in order to isolate the effects of tapering: the IVS was described as a purely elastic, isotropic slab, whereas cardiac tissue is known to show viscoelastic and anisotropic behaviour. These, together with additional curvature in three dimensions, would affect trajectory, attenuation and dispersion of the propagating waves. While these effects were beyond the scope of this study, future work should include them in order to achieve a more reliable model that allows to interpret wave measurements in terms of medium properties.

Finally, it is a known problem[8] that the positioning of the m-line, along which the wave is tracked, can influence the measurement of propagation speed; moreover, it had already been shown that, in the central area of the plate, the A0 and A1 mode would be present simultaneously,[29] which matches our findings. However, we have not been able to find clinical studies in which the choice of placement of the m-line was connected to using knowledge of guided wave behaviour. The results shown in Fig. 2 would suggest that, when tracking ARF-generated waves, it may be beneficial to place the m-line close to one of the surfaces of the septum: in the central region, in fact, there appears to be interference between the A0 and A1 modes, which generates multiple trajectories that can be fitted to identify a propagation speed. Indeed, since the two modes propagate at different speeds, the concept of a single "propagation speed" may be ill defined. On the other hand, it remains to be determined whether other factors, such as viscoelastic effects and anisotropy, play a bigger role in defining the optimal location of the m-line.

5. CONCLUSIONS

In summary, this report presents numerical results on the effects of IVS thickness variations on cardiac SWE measurements.

Our results show that low frequency waves, such as AVC-induced ones, are strongly affected by thickness variation: due to a space-dependent variation in speed, it is not possible to extract a unique value of G from time-space data; moreover, neglecting septal thickness reductions when fitting the dispersion curves can introduce shear modulus estimation errors of up to 30%.

At higher frequencies, typical for ARF-induced waves, the effects of tapering are less pronounced, with no clear deceleration visible in time-space, and small ($< 5\%$) errors coming from overestimating the thickness when fitting the dispersion curves to extract the shear modulus G.

We conclude that the geometry of the septum can affect medium properties estimation performed by SWE, especially when tracking natural waves.

REFERENCES

[1] Joline E. Brandenburg, Sarah F. Eby, Pengfei Song, Heng Zhao, Jeffrey S. Brault, Shigao Chen, and Kai-Nan An. Ultrasound Elastography: The New Frontier in Direct Measurement of Muscle Stiffness. *Archives of Physical Medicine and Rehabilitation*, 95(11):2207–2219, nov 2014.

[2] Lindsey C. Carlson, Timothy J. Hall, Ivan M. Rosado-Mendez, Lu Mao, and Helen Feltovich. Quantitative assessment of cervical softening during pregnancy with shear wave elasticity imaging: an in vivo longitudinal study. *Interface Focus*, 9(5):20190030, oct 2019.

[3] Giovanna Ferraioli, Carmine Tinelli, Barbara Dal Bello, Mabel Zicchetti, Gaetano Filice, and Carlo Filice. Accuracy of real-time shear wave elastography for assessing liver fibrosis in chronic hepatitis C: A pilot study. *Hepatology*, 56(6):2125–2133, dec 2012.

[4] C. Pislaru, M.W. Urban, I. Nenadic, and J.F. Greenleaf. Shearwave dispersion ultrasound vibrometry applied to in vivo myocardium. In *2009 Annual International Conference of the IEEE Engineering in Medicine and Biology Society*, pages 2891–2894. IEEE, sep 2009.

[5] Cristina Pislaru, Matthew W. Urban, Sorin V. Pislaru, Randall R. Kinnick, and James F. Greenleaf. Viscoelastic properties of normal and infarcted myocardium measured by a multifrequency shear wave method: Comparison with pressure-segment length method. *Ultrasound in Medicine and Biology*, 40(8):1785–1795, 2014.

[6] Mihai Strachinaru, Johan G. Bosch, Bas M. van Dalen, Lennart van Gils, Antonius F.W. van der Steen, Nico de Jong, Marcel L. Geleijnse, and Hendrik J. Vos. Cardiac Shear Wave Elastography Using a Clinical Ultrasound System. *Ultrasound in Medicine and Biology*, 2017.

[7] Mihai Strachinaru, Johan G. Bosch, Lennart van Gils, Bas M. van Dalen, Arend F.L. Schinkel, Antonius F.W. van der Steen, Nico de Jong, Michelle Michels, Hendrik J. Vos, and Marcel L. Geleijnse. Naturally Occurring Shear Waves in Healthy Volunteers and Hypertrophic Cardiomyopathy Patients. *Ultrasound in Medicine & Biology*, 45(8):1977–1986, aug 2019.

[8] Lana B.H. Keijzer, Mihai Strachinaru, Dan J. Bowen, Marcel L. Geleijnse, Antonius F.W. van der Steen, Johan G. Bosch, Nico de Jong, and Hendrik J. Vos. Reproducibility of Natural Shear Wave Elastography Measurements. *Ultrasound in Medicine & Biology*, 45(12):3172–3185, dec 2019.

[9] W H Gaasch, H J Levine, M a Quinones, and J K Alexander. Left ventricular compliance: mechanisms and clinical implications. *The American journal of cardiology*, 38(5):645–653, 1976.

[10] Dirk Westermann, Mario Kasner, Paul Steendijk, Frank Spillmann, Alexander Riad, Kerstin Weitmann, Wolfgang Hoffmann, Wolfgang Poller, Matthias Pauschinger, Heinz-Peter Schultheiss, and Carsten Tschope. Role of Left Ventricular Stiffness in Heart Failure With Normal Ejection Fraction. *Circulation*, 117(16):2051–2060, apr 2008.

[11] M. Couade, M. Pernot, E. Messas, A. Bel, M. Ba, A. Hagege, M. Fink, and M. Tanter. In Vivo quantitative mapping of myocardial stiffening and transmural anisotropy during the cardiac cycle. *IEEE Transactions on Medical Imaging*, 30(2):295–305, 2011.

[12] Mathieu Pernot, Wei-Ning Lee, Alain Bel, Philippe Mateo, Mathieu Couade, Mickaël Tanter, Bertrand Crozatier, and Emmanuel Messas. Shear Wave Imaging of Passive Diastolic Myocardial Stiffness. *JACC: Cardiovascular Imaging*, 9(9):1023–1030, sep 2016.

[13] Pengfei Song, Xiaojun Bi, Daniel C. Mellema, Armando Manduca, Matthew W. Urban, James F. Greenleaf, and Shigao Chen. Quantitative Assessment of Left Ventricular Diastolic Stiffness Using Cardiac Shear Wave Elastography. *Journal of Ultrasound in Medicine*, 35(7):1419–1427, jul 2016.

[14] Olivier Villemain, Mafalda Correia, Elie Mousseaux, Jérome Baranger, Samuel Zarka, Ilya Podetti, Gilles Soulat, Thibaud Damy, Albert Hagège, Mickael Tanter, Mathieu Pernot, and Emmanuel Messas. Myocardial Stiffness Evaluation Using Noninvasive Shear Wave Imaging in Healthy and Hypertrophic Cardiomyopathic Adults. *JACC: Cardiovascular Imaging*, 12(7):1135–1145, jul 2019.

[15] Hiroshi Kanai. Propagation of spontaneously actuated pulsive vibration in human heart wall and in vivo viscoelasticity estimation. *IEEE Transactions on Ultrasonics, Ferroelectrics, and Frequency Control*, 52(11):1931–1942, 2005.

[16] Cristina Pislaru, Patricia A. Pellikka, and Sorin V. Pislaru. Wave propagation of myocardial stretch: Correlation with myocardial stiffness. *Basic Research in Cardiology*, 109(6), 2014.

[17] Hendrik J Vos, Bas M van Dalen, Ilkka Heinonen, Johan G Bosch, Oana Sorop, Dirk J Duncker, Antonius F W van der Steen, and Nico de Jong. Cardiac Shear Wave Velocity Detection in the Porcine Heart. *Ultrasound in medicine & biology*, 43(4):753–764, apr 2017.

[18] Pedro Santos, Aniela Monica Petrescu, Joao Pedrosa, Marta Orlowska, Vangjush Komini, Jens-Uwe Voigt, and Jan D'hooge. Natural Shear Wave Imaging in the Human Heart: Normal Values, Feasibility, and Reproducibility. *IEEE Transactions on Ultrasonics, Ferroelectrics, and Frequency Control*, 66(3):442–452, mar 2019.

[19] H. Kanai. 2H-5 Regional Differences in Phase Velocity of Pulsive Wave Propagating Along the Heart Wall. In *2006 IEEE Ultrasonics Symposium*, pages 760–763. IEEE, 2006.

[20] I. Z. Nenadic, M. W. Urban, C. Pislaru, M. Bernal, and J. F. Greenleaf. Fourier Space Analysis of Mechanical Wave Dispersion for Transthoracic in vivo Measurements of Left-Ventricular Viscoelasticity. pages 520–523. 2011.

[21] Naoaki Bekki and Seine A. Shintani. Simple Dispersion Equation Based on Lamb-Wave Model for Propagating Pulsive Waves in Human Heart Wall. *Journal of the Physical Society of Japan*, 84(12):124802, dec 2015.

[22] Hendrik J. Vos, Bas M. van Dalen, Johan G. Bosch, Antonius F.W. van der Steen, and Nico de Jong. Myocardial passive shear wave detection. In *2015 IEEE International Ultrasonics Symposium (IUS)*, pages 1–4. IEEE, oct 2015.

[23] J.L. Rose. *Ultrasonic guided waves in solid media*, volume 9781107048. 2014.

[24] Miguel Bernal, Ivan Nenadic, Matthew W. Urban, and James F. Greenleaf. Material property estimation for tubes and arteries using ultrasound radiation force and analysis of propagating modes. *The Journal of the Acoustical Society of America*, 129(3):1344–1354, mar 2011.

[25] P. H. M. Bovendeerd, J. Rijcken, D. H. Van Campen, A. J. G. Schoofs, K. Nicolay, and T. Arts. Optimization of Left Ventricular Muscle Fiber Orientation. pages 285–296. 1999.

[26] Younho Cho. Estimation of ultrasonic guided wave mode conversion in a plate with thickness variation. *IEEE Transactions on Ultrasonics, Ferroelectrics and Frequency Control*, 47(3):591–603, may 2000.

[27] M.Ech-Cherif El-Kettani, F Luppé, and A Guillet. Guided waves in a plate with linearly varying thickness: experimental and numerical results. *Ultrasonics*, 42(1-9):807–812, apr 2004.

[28] M. E.-C. El-Kettani, M. V. Predoi, and P. Marical. 5K-6 Experimental and Numerical Studies on Lamb Waves Conversion in a Waveguide with Gaussian Section Variation. In *2006 IEEE Ultrasonics Symposium*, pages 1185–1188. IEEE, 2006.

[29] A. Caenen, M. Pernot, D.A. Shcherbakova, L. Mertens, M. Kersemans, P. Segers, and A. Swillens. Investigating shear wave physics in a generic pediatric left ventricular model via in vitro experiments and finite element simulations. *IEEE Transactions on Ultrasonics, Ferroelectrics, and Frequency Control*, 64(2):349–361, 2017.